ISSN 0018-151X, High Temperature, 2018, Vol. 56, No. 2, pp. 239–246. © Pleiades Publishing, Ltd., 2018.
Original Russian Text © K.N. Efimov, V.A. Ovchinnikov, A.S. Yakimov, 2018, published in Teplofizika Vysokikh Temperatur, 2018, Vol. 56, No. 2, pp. 253–260.

HEAT AND MASS TRANSFER AND PHYSICAL GASDYNAMICS

Numerical Study of the Effect of Rotation on the Behavior of the Conjugate Heat and Mass Transfer on the Surface of a Spherically Blunted Cone Exposed to a Hypersonic Flow at an Angle of Attack with Ablation from the Surface

K. N. Efimov, V. A. Ovchinnikov, and A. S. Yakimov*
National Research Tomsk State University, Tomsk, 634050 Russia
**e-mail: yakimovas@mail.ru*
Received May 10, 2016

Abstract—The processes of heating a body in a high-enthalpy spatial flow with allowance for body rotation around its longitudinal axis and ablation of the thermal protection material are studied by means of mathematical simulation. The obtained solution of the problem in conjugate formulation allowed us to take into account the effect of nonisothermic characteristics of the shell on the heat and mass transfer in the boundary layer.

DOI: 10.1134/S0018151X18020074

INTRODUCTION

Aircrafts moving at hypersonic speeds are exposed to the strong thermal action of the atmosphere, which can change their shape and influence their aerodynamic characteristics. Unlike the processes that occur upon axisymmetric heating [1, 2], when a body is exposed to the air flow at an angle of attack, the difference between the heat fluxes on the leeward and windward sides can be significant, inducing a nonuniform heat distribution [3]. To mitigate this effect, hypersonic aircrafts are imparted rotation around their longitudinal axis [4, 5].

Gas flow is described by boundary-layer equations with allowance for laminar and turbulent flows. The system of equations of conservation for a porous medium describes the thermal state of the body. A variety of destruction processes involving the conical section of the body surface and filtration of a coolant gas from pores of the spherical blunting are considered. The development of processes implies the need to solve the problem of aerodynamics in conjugate formulation [6], since it provides an opportunity to improve considerably the accuracy of definition of aerodynamic and thermal characteristics, as compared with separate estimations of aerodynamics, thermochemical destruction, and parameters of motion of the body.

FORMULATION OF THE PROBLEM

Some estimations of relaxation times for gas and condensed phases are presented in [7, 8]. The characteristics of the conjugate heat and mass transfer are obtained on the basis of these results via the solution of the quasi-stationary equations of spatial boundary layer at various flow regimes. The thermal state of the spherical blunting is found by the solution of the nonstationary equation of energy conservation for porous spherical blunting and the quasi-stationary equation for the rate of coolant gas filtering though the pores within the single-temperature model.

Applying the model of chemically equilibrium air and using the hypotheses of "passivity" and the Lewis numbers being unity for all components, we can write a system of equations for the spatial boundary layer in natural coordinate system bound to the external surface of the shell of the body exposed to the flow in the following form [9, 10] (see Fig. 1):

$$\frac{\partial}{\partial s}(\rho u r_w) + \frac{\partial}{\partial n}(\rho v r_w) + \frac{\partial}{\partial \eta}(\rho w) = 0, \tag{1}$$

$$\rho\left(u\frac{\partial u}{\partial s} + v\frac{\partial u}{\partial n} + \frac{w}{r_w}\frac{\partial u}{\partial \eta} - \frac{w^2}{r_w}\frac{\partial r_w}{\partial s}\right) = -\frac{\partial P_e}{\partial s} + \frac{\partial}{\partial n}\left(\mu_\Sigma \frac{\partial u}{\partial n}\right), \tag{2}$$

$$\rho\left(u\frac{\partial w}{\partial s} + v\frac{\partial w}{\partial n} + \frac{w}{r_w}\frac{\partial w}{\partial \eta} + \frac{uw}{r_w}\frac{\partial r_w}{\partial s}\right) = -\frac{1}{r_w}\frac{\partial P_e}{\partial \eta} + \frac{\partial}{\partial n}\left(\mu_\Sigma \frac{\partial w}{\partial n}\right), \tag{3}$$

$$\rho\left(u\frac{\partial H}{\partial s} + v\frac{\partial H}{\partial n} + \frac{w}{r_w}\frac{\partial H}{\partial \eta}\right) = \frac{\partial}{\partial n}\left\{\frac{\mu_\Sigma}{\mathrm{Pr}_\Sigma}\left[\frac{\partial H}{\partial n} + (\mathrm{Pr}_\Sigma - 1)\frac{\partial}{\partial n}\left(\frac{u^2 + w^2}{2}\right)\right]\right\}, \tag{4}$$

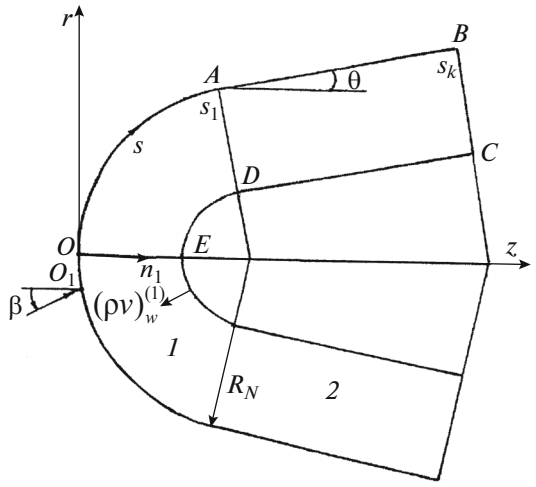

Fig. 1. Schematic image of a flow around the body: (*1*) porous spherical blunting, (*2*) solid conic section of the body.

$$P = \rho h(\gamma_{ef} - 1)/\gamma_{ef}, \quad P = P_e(s,\eta),$$
$$H = h + \left(u^2 + w^2\right)/2, \tag{5}$$

$$\mu_\Sigma = \mu + \Gamma\mu_T, \quad \mathrm{Pr}_\Sigma = \frac{(\mu + \Gamma\mu_T)\,\mathrm{Pr}\,\mathrm{Pr}_T}{\mu\,\mathrm{Pr}_T + \Gamma\mu_T\,\mathrm{Pr}}.$$

For the porous spherical shell ($0 < s < s_1$), assuming the process of injected gas filtration along the normal to the surface in the considered coordinate system bound to the body symmetry axis to be one-dimensional, we obtain [2, 3, 7]:

$$\frac{\partial(\rho_2\varphi v r_1 H_1)}{\partial n_1} = 0, \tag{6}$$

$$(\rho c_p)_1(1-\varphi)\frac{\partial T_1}{\partial t} = \frac{1}{r_1 H_1}\left\{\frac{\partial}{\partial n_1}\left[r_1 H_1 \lambda_1(1-\varphi)\frac{\partial T_1}{\partial n_1}\right]\right.$$
$$\left. + \frac{\partial}{\partial s}\left[\frac{r_1\lambda_1}{H_1}(1-\varphi)\frac{\partial T_1}{\partial s}\right] + \frac{\partial}{\partial \eta}\left[\frac{H_1\lambda_1}{r_1}(1-\varphi)\frac{\partial T_1}{\partial \eta}\right]\right\} \tag{7}$$
$$+ c_{p2}(\rho v)_w^{(1)}\frac{r_{1w}}{r_1 H_1}\frac{\partial T_1}{\partial n_1},$$

$$A\mu v + B\rho_2\varphi v|v| = -\frac{\partial P}{\partial n_1}, \tag{8}$$

$$P = \frac{\rho_2 R T_1}{M}, \quad H_1 = \frac{R_N - n_1}{R_N}, \quad \bar{s} = \frac{s}{R_N},$$
$$r_1 = (R_N - n_1)\sin(\bar{s}), \quad \mu \sim \sqrt{T_1}, \tag{9}$$
$$\lambda_1 \sim \sqrt{T_1}, \quad \varphi = \mathrm{const}.$$

For the conical part of the body ($s_1 < s < s_k$), equations of energy and mass conservation in the moving coordinates are written according to the mathematical models given in [11–13]:

$$\rho_c c_p\left(\frac{\partial T}{\partial t} - \psi\frac{\partial T}{\partial n_1}\right) + c_{p2}G\frac{\partial T}{\partial n_1} = \frac{\partial}{\partial n_1}\left(\lambda\frac{\partial T}{\partial n_1}\right)$$
$$+ \frac{\partial}{\partial s}\left(\lambda\frac{\partial T}{\partial s}\right) + \frac{1}{r_2^2}\frac{\partial}{\partial \eta}\left(\lambda\frac{\partial T}{\partial \eta}\right) - Q_c\frac{d\rho_c}{dt}, \tag{10}$$

$$\frac{d\rho_c}{dt} = \left(\frac{\partial\rho_c}{\partial t} - \psi\frac{\partial\rho_c}{\partial n_1}\right)$$
$$= \begin{cases} -k_c\rho_{c0}\left(\dfrac{\rho_c - \rho_{c*}}{\rho_{c0}}\right)\exp\left(-\dfrac{E_c}{RT}\right), & \rho_c > \rho_{c*}, \\ 0, & \rho_c \le \rho_{c*}, \end{cases} \tag{11}$$

$$G = \int_0^l \frac{d\rho_c}{dt}dn_1, \quad r_2 = (R_N - n_1)\cos\theta + (s - s_1)\sin\theta,$$

$$l = L_0 - x(t), \quad x(t) = \int_0^t \psi d\tau, \quad (\rho v)_{1w} = G_w,$$

$$(\rho v)_w^{(2)} = (\rho v)_{1w} + (\rho v)_{2w} + (\rho v)_{3w}, \quad \psi = \sum_{i=2}^{3}\frac{(\rho v)_{iw}}{\rho_{cw}}. \tag{12}$$

Additionally, the following assumption is made: the typical linear rotation rate of the body is much less than the velocity of the incident flow

$$\Omega = \frac{\omega R_N}{V_\infty} \ll 1. \tag{13}$$

The initial conditions are

$$T_1\big|_{t=0} = T\big|_{t=0} = T_0, \quad \rho_c\big|_{t=0} = \rho_{c0}. \tag{14}$$

The boundary conditions in the gas phase are written as follows: on the exterior boundary of the boundary layer at $n \to \infty$

$$u \to u_e(s,\eta), \quad w \to w_e(s,\eta), \quad h \to h_e(s,\eta), \tag{15}$$

where P_e, u_e, w_e, h_e are found by solving the system of Euler equations [14]; on the surface of the body exposed to the flow at $n = 0$

$$u(s,\eta) = 0, \quad w = w_w, \quad v = v_w. \tag{16}$$

In the case of body rotation, $w_w = \omega r_w$, where ω is the angular rate of rotation from expression (13). For the case without rotation, $w_w = 0$.

On the external surface of the shell ($n = n_1 = 0$), conditions [6] take place at $0 \le \eta < 2\pi$:

$$\frac{\mu}{\mathrm{Pr}}\left(\frac{\partial h}{\partial n}\right)\Big|_w - (1-\varphi)\varepsilon_1\sigma T_{1w}^4 = -\lambda_1(1-\varphi)\left(\frac{\partial T_1}{\partial n_1}\right)\Big|_w, \tag{17}$$
$$0 \le s < s_1,$$

$$-\lambda\frac{\partial T}{\partial n_1}\Big|_{n_1 = 0 - x(t)} = \frac{\mu}{\mathrm{Pr}}\left(\frac{\partial h}{\partial n}\right)\Big|_w - (h_w - h_c)\sum_{i=2}^{3}(\rho v)_{iw}$$
$$- (\rho v)_{1w}(h_w - h_g) - \varepsilon\sigma T_w^4, \quad s_1 \le s \le s_k. \tag{18}$$

On the internal surface of the hemisphere and conical part, the following relations can be written [3, 12]:

$$-\lambda_1(1-\varphi)\frac{\partial T_1}{\partial n_1}\bigg|_{n_1=L_0} = \delta(T_{1,L}-T_0), \quad 0 \le s < s_1, \quad (19)$$

$$\rho_c\Big|_{n_1=l} = \rho_{c0}, \quad \lambda\frac{\partial T}{\partial n_1}\bigg|_{n_1=\ell} = 0, \quad s_1 \le s \le s_k. \quad (20)$$

The ideal contact conditions are assumed on the sphere–cone transition ring $s = s_1$, and the adiabatic condition is used at $s = s_k$

$$\frac{\lambda_1(1-\varphi)}{H_1}\frac{\partial T_1}{\partial s}\bigg|_{s=s_1-0} = \lambda\frac{\partial T}{\partial s}\bigg|_{s=s_1+0},$$
$$T_1\big|_{s=s_1-0} = T\big|_{s=s_1+0}, \quad \frac{\partial T}{\partial s}\bigg|_{s=s_k} = 0. \quad (21)$$

On the external and internal surfaces of the spherical blunting region, the condition of pressure balance inside the pores and in the external environment is applied

$$P_w\big|_{n_1=0} = P_e(s,\eta), \quad P\big|_{n_1=L_0} = P_L. \quad (22)$$

In the absence of the flow symmetry plane, the following periodicity conditions are valid:

$$T_1(t,n_1,s,\eta) = T_1(t,n_1,s,\eta+2\pi),$$
$$T(t,n_1,s,\eta) = T(t,n_1,s,\eta+2\pi). \quad (23)$$

The following kinetic development of nonequilibrium chemical reactions ($T_w \approx 4000$ K) was considered on the boundary surface at $s \ge s_1$ [6, 12]:

$$\mathrm{C}+\mathrm{O}_2 \to \mathrm{CO}_2, \quad 2\mathrm{C}+\mathrm{O}_2 \to 2\mathrm{CO},$$
$$\mathrm{C}+\mathrm{O} \to \mathrm{CO}, \quad \mathrm{C}+\mathrm{CO}_2 \to 2\mathrm{CO},$$
$$2\mathrm{O}+\mathrm{C} \to \mathrm{O}_2+\mathrm{C}, \quad 2\mathrm{N}+\mathrm{C} \to \mathrm{N}_2+\mathrm{C}, \quad (24)$$
$$\mathrm{C} \to \mathrm{C}_1, \quad \mathrm{C} \to \mathrm{C}_3.$$

The molar and mass rates of development of these chemical reactions (24) are detailed in [15], and the ablation rate can be expressed in the following form [12, 15]

$$(\rho v)_{2w} = \rho_w\left[\left(\frac{m_6}{m_2}-1\right)c_{2w}B_1 + \left(2\frac{m_5}{m_2}-1\right)c_{2w}B_2 + \left(\frac{m_5}{m_1}-1\right)c_{1w}B_3 + \left(2\frac{m_5}{m_6}-1\right)c_{6w}B_4\right],$$

$$(\rho v)_{3w} = \sum_{i=7}^{8}\frac{m_i A_{ci}(P_{ci}^* - P_{ci})}{(2\pi R T_w m_i)^{0.5}}, \quad i = 7, 8,$$

$$P_{ci}^* = 10^5\exp(D_i - E_i/T_w), \quad (25)$$

$$B_i = k_{iw}\exp(-E_{iw}/RT_w), \quad i = \overline{1,4},$$
$$P_{ci} = P_e c_{iw}\, m_w/m_i, \quad i = 7,8, \quad \rho_w = P_e m_w/(RT_w),$$

$$h_w = \sum_{i=1}^{8} h_i c_{iw}, \quad m_w^{-1} = \sum_{i=1}^{8} c_{iw}/m_i,$$

$$c_{p2} = b_1 + b_2 T, \quad h_g = \int_0^T c_{p2}\,dT.$$

In Eqs. (24) and (25), the order number of the components corresponds to the following order of their enumeration: $\mathrm{O}, \mathrm{O}_2, \mathrm{N}, \mathrm{N}_2, \mathrm{CO}, \mathrm{CO}_2, \mathrm{C}_1, \mathrm{C}_3$. Here, C designates solid-phase carbon of the thermal protection coating. In the boundary layer, there are four components: $\mathrm{O}, \mathrm{O}_2, \mathrm{N}, \mathrm{N}_2$, which participate in two equilibrium chemical reactions: $\mathrm{O}_2 \leftrightarrow 2\mathrm{O}$, $\mathrm{N}_2 \leftrightarrow 2\mathrm{N}$. There are four components at the condensed gas phase interface: $\mathrm{CO}, \mathrm{CO}_2, \mathrm{C}_1, \mathrm{C}_3$; they are generated in six heterogeneous combustion and sublimation reactions from (24), where two reactions of catalytic recombination of $\mathrm{O}_2, \mathrm{N}_2$ components are also considered.

Let us write balance relations for the component mass concentrations c_{iw} using Fick's law of diffusion and the similar law of thermal and mass transfer [7, 13]:

$$J_{iw} + (\rho v)_w^{(2)} c_{iw} = R_{iw}, \quad i = \overline{1,8},$$
$$J_{iw} = \beta_i(c_{iw} - c_{ie}), \quad \beta_i = \alpha/c_p,$$

where α/c_p and β_i are heat transfer and mass transfer factors, respectively. It is assumed that the products of destruction poorly dilute the air mixture in the boundary layer. This allows the use of the aforementioned formulation for the equations for the boundary layer.

Hereinafter, u, v, w are the components of mean mass rate vector in natural coordinate system (s, n, η); Γ is the alternation factor; H, m are total enthalpy and molecular mass; R_N is the spherical blunting radius; r_w, r_i, $i = 1, 2$, H_1 are Lamé coefficients; h and $(\rho v)_w^{(1)}$ are the enthalpy and the rate of coolant gas outflow from the surface of spherical blunting; $(\rho v)_w^{(2)}$ is the total mass ablation from the carbon surface of the body conical part from the first equation of formula (12); φ is the porosity of the spherical blunting; L_0 is the shell thickness; θ is the cone angle; β is the angle of attack; n_1 is the normal to the surface directed inside the shell; ψ is the linear velocity of displacement of the surface of destruction; R_{iw} are the mass velocities of emergence (disappearance) of the components [15] as a result of heterogenic reactions (24); $x(t)$ is the interface between the gas and condensed phases (the depth of elimination); c_{iw} is the mass concentration of the i-th component; E_{iw}, k_{iw}, $i = 1, \ldots, 4$ are the activation energy and preexponent of the i-th heterogeneous reaction of the shell of the conical part of the body; k_c, E_c and Q_c are the preexponent, activation energy and heat effect of a pyrolytic reaction.

Indices *e*, *eo*, and *w* correspond to the values at the exterior boundary of the boundary layer, at the point of deceleration at the exterior boundary, and on the surface of the body exposed to the flow; subscripts 1 and 2 designate the frame and gas characteristics on the sphere; *g* presents the gas phase on the conical part of the surface; ∞ corresponds to the parameters of incident gas flow at the infinity; *T*, 0 designate parameters of turbulent transport and initial conditions; *L* corresponds to the internal shell of the spherical part of the body; *k* marks the peripheral section of the shell; superscripts 1 and 2 correspond to the parameters of the coolant flow rate on the porous hemisphere and surface chemical reactions on the conical part of the body; the overbar relates to the dimensionless parameters, *z* is associated with the time of termination of the heat impact; ef denotes the effective value, *st* designates steel, *tu* marks tungsten, and *c* refers to carbon-fiber reinforced plastic.

METHOD OF CALCULATION AND INPUT DATA

The system of equations (1)–(4), (6)–(8), (10), and (11) subject to initial and boundary conditions (14)–(23) is solved numerically. The system of equations for a spatial boundary layer is solved in the Dorodnitsyn variables with allowance for laminar, transitional, and turbulent flows. The two-layer of turbulent boundary layer model is applied to describe the turbulent flow [16, 17]. The considered three-layer algebraic turbulence model allows for a laminar viscous sublayer, a turbulent internal core described by the Van-Driest-Cebeci formula [17], and an exterior space where the Spalding formula [16] is used. The transition point is chosen proceeding from the supposition that at the given pressure and enthalpy of drag action the maximum heat flux is located near the sound line of the spherical blunting. The alternation coefficient and the laminar–turbulent transition are described by the Dhawan–Narasimha formula [18]. At numerical integration, $\mathrm{Pr} = 0.72$, $\mathrm{Pr}_T = 1$. The iteration and interpolation method [19] is applied to the boundary layer equations to obtain combined difference schemes aimed at merging of the sought characteristics at the interface between the laminar sublayer and the turbulent core and considering μ_T behavior across the boundary layer. Tests of this boundary layer model by comparing with the experimental results of [20, 21] show its good applicability.

The numerical solution of three-dimensional equations (7) and (10) was performed by the decomposition method [22]. An implicit, absolutely stable, monotone difference scheme with the aggregate approximation error $O(\tau + H_{n_1}^2 + H_s^2 + H_\eta^2)$, was used, where H_{n_1}, H_s, H_η were spatial steps along coordinates n_1, *s*, and η, respectively; τ was the time step. To estimate the numerical error of the results in the porous body, the sequence of grids condensed in space was used: $h_1 = h_{n_1} = 10^{-3}$ m, $h_2 = h_{s1} = 0.925 \times 10^{-2}$ (on the sphere), $h_3 = h_{s2} = 10^{-2}$ (on the cone), $h_4 = h_\eta = 0.087$. The following parameters were taken: $H_{1,i} = 2 \times h_i$, $H_{2,i} = h_i$, $H_{3,i} = h_i/2$, $H_{4,i} = h_i/4$, $i = 1$–4. The temperature of the frame was fixed along the body thickness at various times. In all cases, the problem is solved with a variable time step subject to the condition of accuracy, which is set the same for all spatial steps. The difference between the values of the relative temperature error decreased and by time $t = t_z$ was $\Delta_1 = 11.2\%$, $\Delta_2 = 6.3\%$, and $\Delta_3 = 3.1\%$. The results presented below were obtained for spatial steps $H_{3,i} = h_i/2$, $i = 1$–4.

The results of theoretical [23] and generalized experimental researches [24] were used to test the interaction of high-enthalpy airflows with graphite surfaces.

The quasi-stationary continuity equation (6) $(\rho v)_w^{(1)} r_{1w}/(H_1 r_1) = -\rho_2 \varphi v$ (minus is stipulated by the normal coordinate n_1 directed inward the body (see Fig. 1) with the coolant flowing in the opposite direction) together with the first expression (9), nonlinear Darcy's law (8) and boundary conditions (22) can be integrated to find the gas flow rate and pressure in area *1* [3]:

$$(\rho v)_w^{(1)}(s,\eta) = \frac{\left[2B(P_L^2 - P_w^2)\varphi M D_L/R + E_L^2\right]^{0.5} - E_L}{2BD_L}, \quad (26)$$

$$P(n_1,s,\eta) = \{P_w^2 + 2R(\rho v)_w [B(\rho v)_w D + E]/M\varphi\}^{0.5},$$

where $D(n_1,s,\eta) = \int_0^{n_1} T_1 \left(\frac{r_{1w}}{r_1 H_1}\right)^2 dy$,

$$E(n_1,s,\eta) = A\int_0^{n_1} \mu T_1 \frac{r_{1w}}{r_1 H_1} dy.$$

The pressure on the internal "cold" surface of blunting *L* is given in the form of

$$P_L = kP_{e0}, \quad (27)$$

where *k* is a certain constant. This ensures the necessary flow rate of the coolant (in particular, the melting point of the frame made of foamed metals was not reached [13, 25]) within the section of thermal action from $t = 0$ to $t = t_z$.

Calculations of the chemically balanced airflow around the spherically blunted cone with half the apex angle $\theta = 10°$ at angle of attack $\beta = 5°$ were carried out in conditions [14], corresponding to parameters: $V_\infty = 7000$ m/s, $R_N = 0.2$ m, $L_0 = 0.02$ m. Kinetic constants (25) of heterogeneous reactions (24) are taken from [7], and graphite enthalpy h_c is calculated by formula given in [26]. The effective adiabat γ_{ef} in the first for-

mula (5) is obtained according to [14]. Thermal and physical data for carbon material of the conical shell are presented in [12], data for foamed steel are given in [27], and those for tungsten are in [28]. For graphite of the conical part, eq. (10) is solved at $Q_c = 0$, and $G = 0$.

The results given below are obtained at $h_{e0} = 2.47 \times 10^7$ J/kg, $\varphi = 0.34$, $T_0 = 300$ K, $b_1 = 965.5, b_2 = 0.147$, $M = 29$ kg/kmol, $\sigma = 5.67 \times 10^{-8}$ W/(m^2 K^4), $\varepsilon = 0.9$, $P_0 = 10^5$ N/m^2, $\rho_{c0} = 1400$ kg/m^3, $\rho_{c*} = 1300$ kg/m^3, $\rho_{tu} = 19300$ kg/m^3, $k_c = 3.15 \times 10^6$ s^{-1}, $E_c = 8.38 \times 10^4$ J/mol, $Q_c = 1.26 \times 10^6$ J/kg, $t_z = 40$ s. The thermal and physical characteristics of the porous blunting correspond to foamed steel $\varepsilon_1 = 0.8$, $\lambda_1 = 2.92 + 4.5 \times 10^{-3} T_1$ W/(m K), $\rho_1 c_{p1} = (1252 + 0.544 T_1) \times 10^3$ J/(K m^3) [27], $A = 2.3 \times 10^{11}$ L/m^2, $B = 5.7 \times 10^5$ L/m and permeable tungsten $\varepsilon_1 = 0.3$, $A = 3.03 \times 10^{14}$ L/m^2, $B = 6.1 \times 10^8$ L/m [29]. The thermal and physical characteristics of the conical part of the body correspond to carbon-fiber reinforced plastic [12] or solid graphite V-1 [30].

RESULTS OF NUMERICAL SOLUTION AND THEIR ANALYSIS

In Figs. 2–4, the temperature of the body surface along the contour is presented as a function of longitudinal coordinate $\bar{s}$ in cross sections of azimuthal coordinate $\eta = 0 - \pi$ for composite materials: foamed steel–carbon-fiber reinforced plastic (Fig. 2), permeable steel–graphite V-1 (Fig. 3), foamed tungsten–graphite V-1 (Fig. 4).

Curves *1–4* in Figs. 2–4 refer to times t: 0 (*1*), 1 (*2*), 5 (*3*), t_z (*4*) ($t_z = 40$ s corresponds to the stationary regime of the body heating). Solid curves in Figs. 2–4 are plotted for cases without rotation, and dashed curves are for $\Omega = 0.00027$ ($\omega = 8.827$ rad/s). The results in Figs. 5–9 are shown for $t = t_z$.

The curves in Fig. 2 show the coolant gas flow rate $(\rho v)_w^{(1)}$ from (26), curve *1* in Fig. 5 at $H = 2.5 \times 10^4$ m, $P_{e0} = 18.93 \times 10^5$ N/m^2, $T_{e0} = 8005$ K and $k = 1.1$ from formula (27). Surface temperature curves (Fig. 3) show $(\rho v)_w^{(1)}$ for number *2* in Fig. 5 obtained at $H = 2.2 \times 10^4$ m, $P_{e0} = 30.44 \times 10^5$ N/m^2, $T_{e0} = 8205$ K and $k = 1.1$. Value of $(\rho v)_w^{(1)}$ for number *3* in Fig. 5 obtained at $H = 1.8 \times 10^4$ m, $P_{e0} = 57.35 \times 10^5$ N/m^2, $T_{e0} = 8535$ K and $k = 20$ refers to tungsten (Fig. 4).

In these cases, the distribution of the required pressure P_L in the chamber for spherical bluntings made of foamed metals can be selected such that the temperature of blunting over the entire section of heating remains lower than the melting point until $t_z = 40$ s.

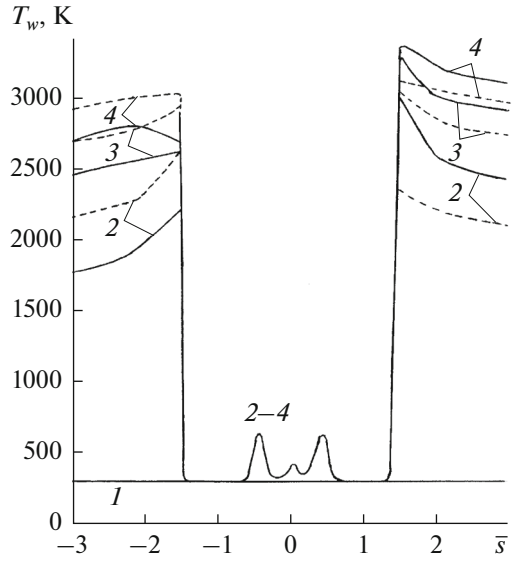

Fig. 2. Surface temperature distribution over the contour of section $\eta = 0–\pi$ for foamed steel–carbon-fiber reinforced plastic composite material at times t: (*1*) 0, (*2*) 1, (*3*) 5, (*4*) t_z.

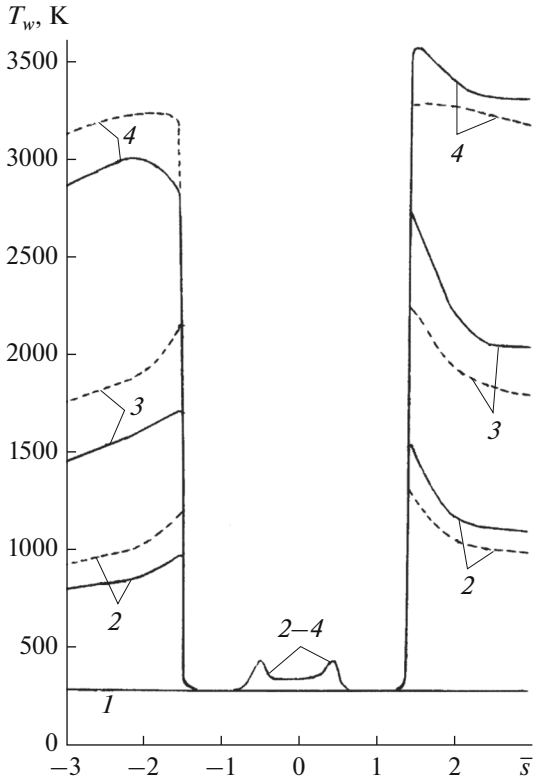

Fig. 3. Surface temperature distribution over the contour of section at $\eta = 0–\pi$ for permeable steel–graphite V-1 composite material. The denotations are the same as in Fig. 2.

As Figs. 2–4 show, at $\omega \neq 0$ (dashed curves), the observed drop of the surface temperature on the windward side and its increase on the leeward side is caused by a heat overflow induced by the body rotation. Note that, when the data for tungsten from [28] is used, much greater pressure drops between the chamber and

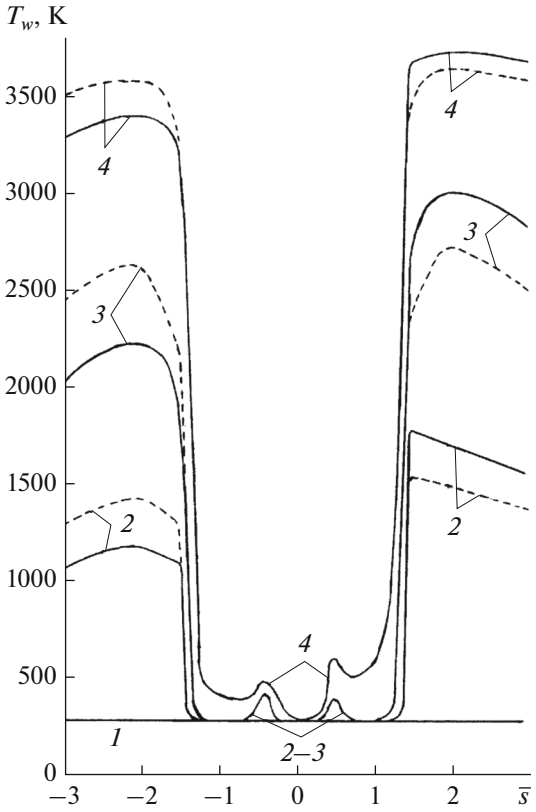

Fig. 4. Surface temperature distribution over the contour of section $\eta = 0–\pi$ for foamed tungsten–graphite V-1. The denotations are the same as in Fig. 2.

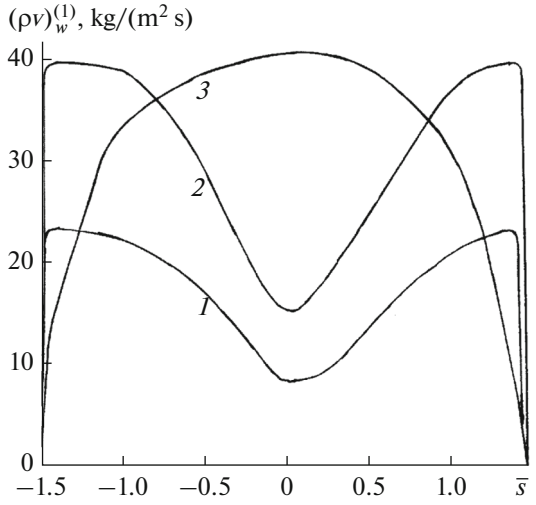

Fig. 5. Distribution of the coolant gas mass flow rate over the contour of the spherical blunting at $t = t_z$: (*1*) foamed steel–carbon-fiber reinforced plastic, (*2*) permeable steel–graphite V-1, (*3*) foamed tungsten–graphite V-1.

the spherical blunting contour are required to prevent melting. For the steady-state temperature regime, the effect of heat overflow is manifested both in the body conical section bordering upon the spherical blunting and in its spherical part. With increasing intensity of injection into the region of spherical blunting (see

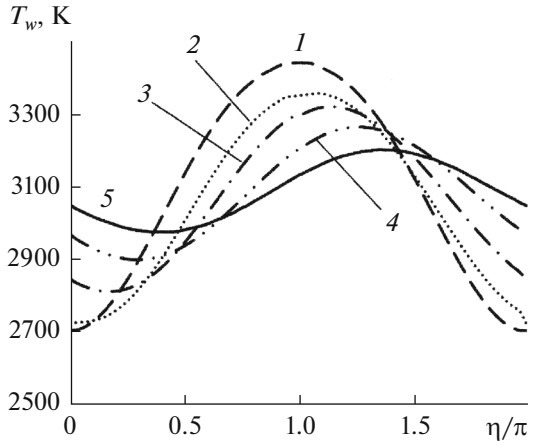

Fig. 6. Distribution of the surface temperature over the body conic section (carbon-fiber reinforced plastic) along the azimuthal coordinate in the section of longitudinal coordinate $\bar{s} = 9.08$, rotation rates: (*1*) 0°/s, (*2*) 25, (*3*) 100, (*4*) 250, and (*5*) 500.

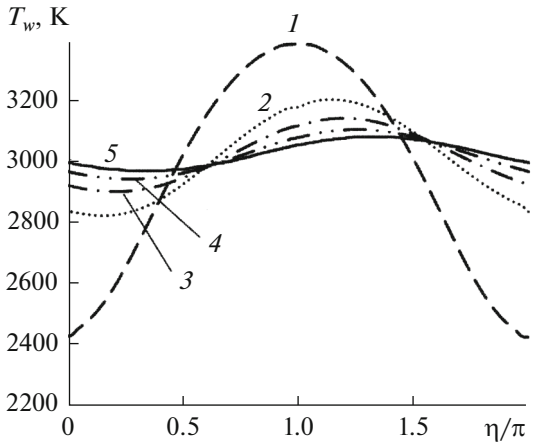

Fig. 7. Distribution of the surface temperature over the body conic section (graphite V-1) along the azimuthal coordinate in section $\bar{s} = 9.08$. The denotations are the same as in Fig. 6.

curve *3* in Fig. 5) the equilibrium temperature decreases and initiates the regime of heat sink from the body conical section to its spherical part if the used materials possess high thermal conductivity (see curves *4* in Fig. 4 for tungsten). Additionally, heat absorption occurs when gas is filtered through the pores of spherical blunting.

The temperatures of the interior wall of the spherical blunting, which is $T_{st} = 300$ K for permeable steel and $T_{tu} = 341$ K for foamed tungsten at $t_z = 40$ s, is of practical interest. As for carbon-fiber reinforced plastic, by t_z, the temperature of the internal wall of the body conical section made of it did not exceed $T_c = 310$ K.

In Figs. 6–7, the surface temperature distributions along the azimuthal coordinate in the longitudinal coordinate section $\bar{s} = 9.08$ (conic part of the body) are presented at $H = 2.2 \times 10^4$ m, $P_{e0} = 30.44 \times 10^5$ N/m^2,

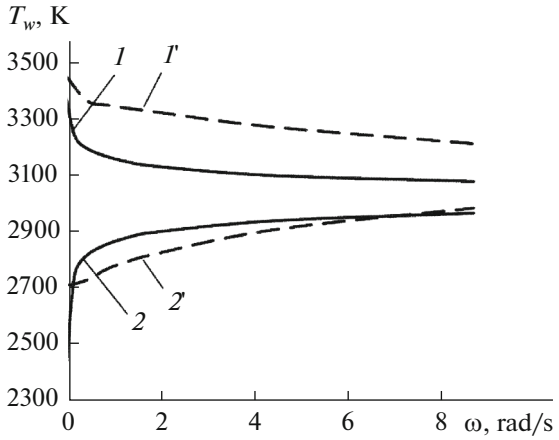

Fig. 8. Surface temperature of the body conic section as a function of rotation rate in section $\bar{s} = 9.08$.

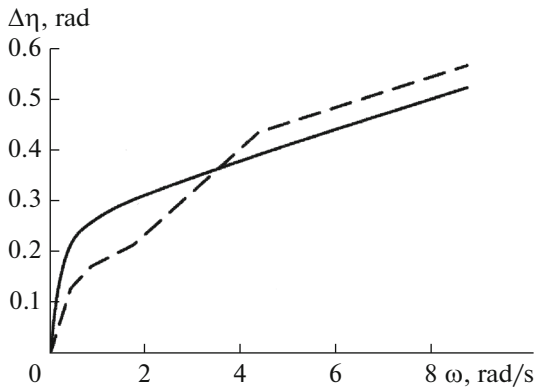

Fig. 9. Shift of maximum temperature of the surface relative to coordinate $\eta = \pi$ as a function of rotation rate. The dashed curve is carbon-fiber reinforced plastic, and the solid curve is graphite V-1.

$T_{e0} = 8205$ K, and $k = 1.1$, for the following materials: foamed steel–carbon-fiber reinforced plastic (Fig. 6), permeable steel–graphite V-1 (Fig. 7). Curves *1–5* show rotation rates of 0, 25, 100, 250 and 500°/s. It is shown that the maximum temperature of the body decreases and its minimum increases with the increase in rotation rate; i.e., the temperature gradient declines. The temperature peaks are shifted along the direction of body rotation.

The rotation influence on the drop of the body surface temperature at input data from Fig. 6 in the longitudinal coordinate section $\bar{s} = 9.08$ is shown in Fig. 8. The data for graphite V-1 are mapped by solid curves, and those for carbon-fiber reinforced plastic are shown by dashed curves. Curves *1–1'* show the maximum surface temperature, and curves *2–2'* correspond to the minimum surface temperature. It is shown that, with an increase in rotation rate, the temperature drop decreases. The influence of the rotation rate variations on the surface temperature drop is different for graphite and carbon-fiber reinforced plastic: at the rate increase from 0 to 25°/s (0.436 rad/s) the temperature drop reduces from 947 to 379 K for graphite, and from 742 to 635 K for carbon-fiber reinforced plastic. The latter effect is apparently related to the fact that thermal conductivity of graphite which is much higher than that of carbon-fiber reinforced plastic [12, 30]. With the increase in the rotation rate, its effect on the body surface temperature decreases. At $\omega = 250$°/s, the temperature drop for graphite and carbon-fiber reinforced plastic is 162 and 368 K, and at $\omega = 500$°/s, it is 113 and 229 K, respectively. This indicates that the greatest effect is produced by rotation at low ω. At the same time, thermal protection materials with low thermal conductivity need higher rotation rates to reach the temperature gradients typical for heat-conducting materials.

In Fig. 9, the maximum surface temperature displacement relative to the azimuthal coordinate $\eta = \pi$ (winward side) is presented as a function of the rotary speed. This displacement determined with the accuracy of a mesh point along the azimuthal coordinate η reveals the asymmetry of the thermal field on the thermal protection surface, which induces the asymmetry of the flow around the body rotating relative to the plane of the angle of attack. Consequently, the emerging negative roll moment decelerates the body rotation, and the lateral force deflects the body from the set trajectory. This should be taken into consideration when a suitable rotation rate is chosen. It is shown that at $\omega > 250$°/s (4.36 rad/s) the displacement for carbon-fiber reinforced plastic (dotted curve) grows faster than for graphite (solid curve).

CONCLUSIONS

The conjugate formulation of the problem allows consideration of the influence of nonisothermic characteristics of the shell walls on the heat and mass transfer in the boundary layer.

The influence of body rotation on heat overflow in the thermal protection shell was evaluated. It was shown that, by the selection of thermal protection material and the rate of rotation around its longitudinal axis, we can manage the modes of heat and mass transfer in a body moving at a supersonic velocity.

REFERENCES

1. Bashkin, V.A. and Reshet'ko, S.M., *Uch. Zap. Tsentr. Aerogidrodin. Inst.*, 1989, vol. 20, no. 5, p. 53.
2. Zinchenko, V.I., Kataev, A.G., and Yakimov, A.S., *J. Appl. Mech. Tech. Phys.*, 1992, vol. 33, no. 6, p. 821.
3. Zinchenko, V.I. and Yakimov, A.S., *J. Appl. Mech. Tech. Phys.*, 1999, vol. 40, no. 4, p. 607.
4. Markov, A.A., *Fluid Dyn.*, 1984, vol. 19, no. 3, p. 499.
5. Krasilov, N.A., Levin, V.A., and Yunitskii, S.A., *Fluid Dyn.*, 1986, vol. 21, no. 1, p. 90.
6. Zinchenko, V.I., Efimov, K.N., and Yakimov, A.S., *High Temp.*, 2007, vol. 45, no. 5, p. 681.

7. Grishin, A.M. and Fomin, V.M., *Sopryazhennye i nestatsionarnye zadachi mekhaniki reagiruyushchikh sred* (Conjugate and Nonstationary Problems of the Mechanics of Reacting Media), Novosibirsk: Nauka, 1984.
8. Grishin, A.M. and Zinchenko, V.I., *Fluid Dyn.*, 1974, vol. 9, no. 2, p. 263.
9. Zinchenko, V.I., *Matematicheskoe modelirovanie sopryazhennykh zadach teplomassoobmena* (Mathematical Modeling of Coupled Heat and Mass Transfer Problems), *Tomsk*: Tomsk. Gos. Univ., 1985.
10. Shevelev, Yu.D., *Trekhmernye zadachi teorii laminarnogo pogranichnogo sloya* (Three-Dimensional Problems of the Laminar Boundary Layer Theory), Moscow: Nauka, 1977.
11. Gorskii, V.V. and Zaprivoda, A.V., *High Temp.*, 2014, vol. 52, no. 2, p. 230.
12. Grishin, A.M., Parashin, A.D., and Yakimov, A.S., *Combust., Explos. Shock Waves (Engl. Transl.)*, 1993, vol. 29, no. 1, p. 82.
13. Polezhaev, Yu.V. and Yurevich, F.P., *Teplovaya zashchita* (Thermal Protection), Moscow: Energiya, 1976.
14. Lunev, V.V., Magomedov, K.M., and Pavlov, V.G., *Giperzvukovoe obtekanie prituplennykh konusov s uchetom ravnovesnykh fiziko-khimicheskikh prevrashchenii* (Hypersound Flow around Blunted Cones with Allowance for Equilibrium Physical and Chemical Transformations), Moscow: Vychisl. Tsentr Akad. Nauk SSSR, 1968.
15. Stepanova, E.V. and Yakimov, A.S., *High Temp.*, 2015, vol. 53, no. 2, p. 228.
16. Patankar, S.V. and Spalding, D.B., *Heat and Mass Transfer in Boundary Layers*, London: Morgan–Grampian, 1967.
17. Cebeci, T., *AIAA J.*, 1970, vol. 8, no. 12, p. 48.
18. Kovalev, V.L., *Geterogennye kataliticheskie protsessy v aerotermodinamike* (Heterogeneous Catalytic Processes in Aerothermodynamics), Moscow: Fizmatlit, 2002.
19. Grishin, A.M., Zinchenko, V.I., Efimov, K.N., Subbotin, A.N., and Yakimov, A.S., *Iteratsionno-interpolyatsionnyi metod i ego prilozheniya* (Iteration–Interpolation Method and Its Applications), *Tomsk*: Tomsk. Gos. Univ., 2004.
20. Feldhuhn, R.N., Heat transfer from a turbulent boundary layer on a porous hemisphere, *AIAA Pap.* 76-119, 1976.
21. Widhopf, G.F. and Hall, R., *AIAA J.*, 1972, vol. 10, p. 1318.
22. Samarskii, A.A., *Vvedenie v teoriyu raznostnykh skhem* (Introduction to the Theory of Difference Schemes), Moscow: Nauka, 1971.
23. Gofman, A.G. and Grishin, A.M., *J. Appl. Mech. Tech. Phys.*, 1984, vol. 25, no. 4, p. 598.
24. Baker, R.L., *AIAA J.*, 1977, vol. 15, p. 1391.
25. Andrievskii, R.A., *Poristye metallokeramicheskie materialy* (Porous Metal-Ceramic Materials), Moscow: Metallurgiya, 1964.
26. Buchnev, L.M., Smyslov, A.I., Dmitriev, I.A., et al., *Teplofiz. Vys. Temp.*, 1987, vol. 25, no. 6, p. 1120.
27. Alifanov, O.M., Tryanin, A.P., and Lozhkin, A.L., *J. Eng. Phys.*, 1987, vol. 52, no. 3, p. 340.
28. Zinov'ev, V.F., *Teplofizicheskie svoistva metallov pri vysokikh temperaturakh. Spravochnik* (Thermophysical Properties of Metals at High Temperatures: A Reference Book), Moscow: Metallurgiya, 1989.
29. Kurshin, A.P., *Tr. Tsentr. Aerogidrodin. Inst.*, 1984, no. 2230, p. 10.
30. Sosedov, V.P., *Svoistva konstruktsionnykh materialov na osnove ugleroda. Spravochnik* (Properties of Carbon-Based Structural Materials: A Reference Book), Moscow: Metallurgiya, 1975.

Translated by N. Semenova